# Discrete Memristor Hyperchaotic Maps

Han Bao, Zhongyun Hua, *Member, IEEE*, Houzhen Li, *Graduate Student Member, IEEE*, Mo Chen, *Member, IEEE*, and Bocheng Bao, *Member, IEEE*

***Abstract*— Regarding as a basic circuit component with special nonlinearity, memristor has been widely applied in chaotic circuits and neuromorphic circuits. However, discrete memristor (DM) has not been received much attention, yet. To this end, this paper reports a general DM model and its unified mapping model. Using the general DM model, four representations of DMs are given and their pinched hysteresis loops are exhibited. Based on the unified DM mapping model, four two-dimensional (2D) DM maps are generated and their parameter-relied and initials-relied behaviors are explored using multiple numerical measures. The results demonstrate that all the four 2D DM maps can generate hyperchaos with coexisting bi-stable or memristor initial-boosted behavior, and their sequences have excellent performance indictors. A hardware device is constructed to implement these maps and the analog voltage signals are experimentally acquired. Moreover, pseudo-random number generators (PRNGs) are designed using these DM maps and the test results show that the generated pseudo-random numbers (PRNs) have high randomness.**

***Index Terms*— Discrete map, discrete memristor, hardware device, hyperchaos, initial, pseudo-random number (PRN).**

## I. Introduction

BOTH continuous and discrete dynamical systems can exhibit chaotic behaviors with some specific parameters and initial values [1], [2]. A dynamical system is chaotic if it has the properties of initial sensitivity, topological transitivity, track ergodicity and random similarity. With these properties, chaotic systems are widely studied and used in academic and industrial fields [3]–[5]. In order to generate chaos, a dynamical system should contain one or more nonlinear functions. The polynomial function, absolute value function, trigonometric function, and exponential function are several general nonlinearities, and they play a particularly important role in generating chaos. But these nonlinearities don't have any internal state variables. Regarding as a basic circuit component, memristor possesses a special nonlinearity due to its built-in internal state variable [6] and it is essentially different from the general nonlinearity [7], [8]. Due to the special nonlinearity [9] and synaptic plasticity [10], [11], memristors have been widely applied in chaotic circuits and neuromorphic circuits.

Since the hyperchaos has more than one positive Lyapunov exponent and it is a much more complex behavior than the chaos, the hyperchaotic systems can achieve high security level for many chaos-based applications such as the secure communication [12]. Generally speaking, to produce hyperchaos, the continuous dynamical system needs at least four dimensions [13], [14], while the discrete dynamical system needs only two [15], [16]. For example, the memristor-based continuous systems cannot achieve hyperhcaos when they only have three dimensions in the $(\varphi, q)$-domain [17], and can generate hyperchaos when they have four dimensions in the $(\upsilon, i)$-domain [13], [14]. As a contrast, many 2D memristor-based discrete maps can generate hyperchaos with excellent performance [16], [18], [19]. Thus, compared with the continuous systems, the discrete systems usually have simpler algebraic equations [20] and higher computational efficiency in chaos-based industrial applications [21]. However, except for a few 2D designated discrete maps, including the sine chaotification map [15], sine Logistic modulation map [22], and sine boostable map [20], most existing 2D discrete maps cannot show hyperchaotic oscillations [23]–[27]. As a result, to achieve hyperchaos in discrete maps with simple algebraic equations is an interesting research topic.

Mathematical modeling is an important technique to theoretically analyze, numerically simulate and experimentally observe the memristor devices and their constituent systems. Some commonly used memristor modeling methods include physical device modeling [28], SPICE simulation modeling [29], [30], and equivalent circuit modeling [31]. However, most of these existing memristor model methods are in the continuous time domain. For example, the HP $TiO_2$ memristor reported in [28] is a physical device and its linear drift model is a continuous model in mathematics. When the continuous memristor model is used in discrete systems or digital circuits, it may lead to poor controllability and unrepeatability. The discrete memristor model constructed in the discrete domain can well address the above issues of the continuous memristor model. Therefore, the discrete memristor model, referred to as discrete memristor (DM), is more conducive to the research and application of memristor in discrete systems and digital circuits than the continuous memristor model.

Manuscript received December 15, 2020; revised February 18, 2021 and April 11, 2021; accepted May 19, 2021. Date of publication June 4, 2021; date of current version November 9, 2021. This work was supported by the National Natural Science Foundation of China under Grant 51777016 and Grant 62071142. This article was recommended by Associate Editor Z. Zeng. *(Corresponding authors: Bocheng Bao; Zhongyun Hua.)*

Han Bao, Houzhen Li, Mo Chen, and Bocheng Bao are with the School of Microelectronics and Control Engineering, Changzhou University, Changzhou 213164, China (e-mail: charlesbao0319@gmail.com; leehzh@126.com; mchen@cczu.edu.cn; mervinbao@126.com).

Zhongyun Hua is with the School of Computer Science and Technology, Harbin Institute of Technology, Shenzhen, Shenzhen 518055, China (e-mail: huazyum@gmail.com).

Color versions of one or more figures in this article are available at https://doi.org/10.1109/TCSI.2021.3082895.

Digital Object Identifier 10.1109/TCSI.2021.3082895

Recently, a DM model was first established using forward Euler difference method and a novel 2D hyperchaotic map was derived from a sampling switch-based memristor-capacitor circuit [18]. More recently, our previous work first proposed a discrete charge-controlled memristor with cosine memductance and then constructed a general frame for 2D memristive maps by coupling the DM with some one-dimensional (1D) discrete maps [19]. Based on the general frame, four 2D memristive hyperchaotic maps were thereby provided by employing three existing 1D discrete maps and one 1D linear discrete map. The results demonstrated that the DM can greatly improve the chaos complexity of the existing 1D discrete map. Inspired by these tentative ideas, this paper reports a general DM model and its unified mapping model. Different from only one DM model in [19], four DM models are provided in this paper. Particularly, by presenting a simplest schematic structure, four examples of 2D DM maps using different memristance nonlinearities are presented in terms of the unified DM mapping model.

The presented four 2D DM maps can generate hyperchaos with the excellent performance and two of them can show the memristor initial-boosted behaviors. In particular, such the memristor initial-boosted behaviors make the offset-boosted hyperchaotic sequences own the same performance indicators [20], which mean that their oscillating amplitudes can be non-destructively controlled by switching the memristor initials. In other words, when the memristor initials are periodically switched, the performance indicators of the hyperchaotic sequences remain unchanged, but their oscillating amplitudes are limited to different dynamic ranges [20]. This feature is very important for some chaos-based industrial applications [19] and most existing discrete maps don't have this feature [2]. So designing simple hyperchaotic maps using the DMs is a novel research topic. Furthermore, we develop a hardware device with analog voltage outputs to implement the four 2D DM maps and design a PRNG using these hyperchaotic maps to explore their application [19]. The experimental results show the easy implementation of these DM maps and the high randomness of the generated PRNs.

The contributions of this paper are summarized as follows. (1) A general DM model is proposed and four representations of DMs with different memductance nonlinearities are given. (2) A unified DM mapping model is presented and four 2D DM hyperchaotic maps with infinite fixed points are provided. (3) The memristor initial-boosted behaviors are studied and the hyperchaotic sequences can be non-destructively controlled by switching the memristor initials. (4) A hardware device is developed to implement these maps and a PRNG is designed to explore the application.

The rest of this paper is organized as follows. Section II reports a general DM model and its unified mapping model. Section III provides four 2D DM maps and investigates their complex behaviors. Section IV evaluates the performance indicators of the hyperchaotic sequences and develops a hardware device to acquire the analog voltage signals. Section V applies the hyperchaotic sequences to a PRNG. Finally, this paper is concluded in Section VI.

## II. General DM Model and Its Mapping Model

This section reports a DM in a general form and its unified mapping model. With such a mapping model, four examples of 2D DM maps are presented and their basic dynamics are discussed.

### A. General DM Model and Four DMs

From the perspective of circuit theory, memristor is a two-terminal nonlinear device. When applying any periodic voltage or current stimulus, the memristor displays a pinched hysteresis loop in the plane of voltage $v(t)$ and current $i(t)$. According to the definition of memristor in [9], an ideal charge-controlled memristor is given by

$$\begin{aligned} v(t) &= M(q)i(t), \\ \mathrm{d}q(t)/\mathrm{d}t &= i(t), \end{aligned} \tag{1}$$

where $q$ stands for the charge variable and $M(q)$ represents the memristance in Ohms.

The continuous memristor in (1) can be discretized using forward Euler difference method [18], [19]. Let $v_n$, $i_n$, and $q_n$ be the sampling values of $v(t)$, $i(t)$, and $q(t)$ at the $n$-th iteration, respectively, and $q_{n+1}$ be the sampling value of $q(t)$ at the $(n+1)$-th iteration. Then, an ideal DM can be modeled by

$$\begin{aligned} v_n &= M(q_n)i_n, \\ q_{n+1} &= q_n + i_n, \end{aligned} \tag{2}$$

where $M(q_n)$ represents the sampling value of memristance $M(q)$ at the $n$-th iteration.

According to the mathematical representations of continuous memristors used in [1], [32], [33], four representations of DMs with different memductance nonlinearities can be generated as

$$\text{Quadratic DM (Q-DM)}: M(q_n) = q_n^2 - 1, \tag{3a}$$

$$\text{Absolute value DM (A-DM)}: M(q_n) = |q_n| - 1, \tag{3b}$$

$$\text{Sinusoidal DM (S-DM)}: M(q_n) = \sin(\pi q_n), \tag{3c}$$

$$\text{Exponential DM (E-DM)}: M(q_n) = \mathrm{e}^{-\cos \pi q_n} - 1. \tag{3d}$$

Note that since $M(q_n) = \cos(\pi q_n)$ mentioned in the literature [18], [19] has similar properties to $M(q_n) = \sin(\pi q_n)$ given in (3c), we omit it here. Thus, four DMs can be generated and they all have simple mathematical models.

By referring to the test scheme reported in [9], we connect a discrete current source across the input terminals of the aforementioned four DMs respectively. Denote the discrete current as $i_n = 0.02\sin(\omega n)$ A ($\omega$ is radian frequency). When applying the discrete current to these four DMs, their properties can be demonstrated in the $i_n - v_n$ plane using MATLAB numerical simulations [19]. For different values of $\omega$ with fixed memristor initial $q_0 = 0$ C, the constitutive voltage-current relations are obtained and depicted in Fig. 1. As can be seen, all the four DMs can exhibit the frequency-relied hysteresis loops pinched at the origin and their hysteresis loop lobe areas decrease monotonically with the increasement of the radian frequency $\omega$. Meanwhile, for different values

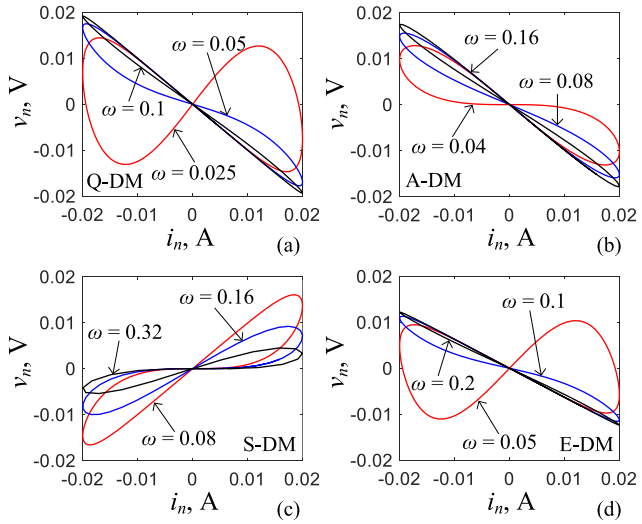


Fig. 1. Frequency-relied pinched hysteresis loops of four DMs when applying a discrete current source $i_n = 0.02\sin(\omega n)$ A, where the memristor initial is fixed as $q_0 = 0$ C and different radian frequencies of $\omega$ (rad/s) are given in the diagram. (a) Q-DM. (b) A-DM. (c) S-DM. (d) E-DM.

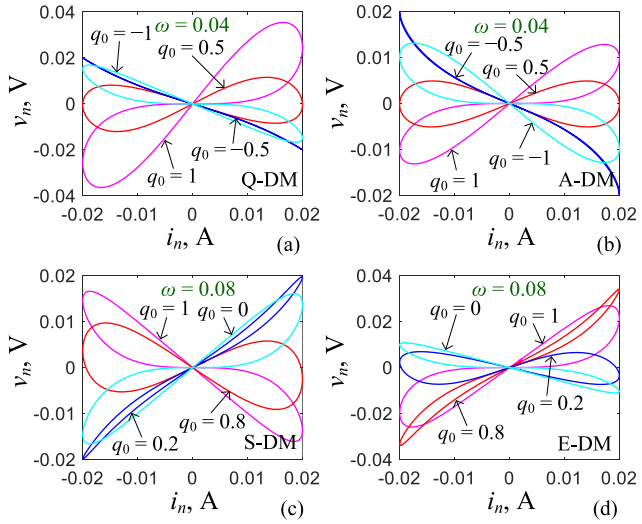


Fig. 2. Initial-relied pinched hysteresis loops of four DMs when applying a discrete current source $i_n = 0.02\sin(\omega n)$ A, where the memristor initial $q_0$ (C) and radian frequency $\omega$ (rad/s) are given in the diagram. (a) Q-DM. (b) A-DM. (c) S-DM. (d) E-DM.

of memristor initial $q_0$ with fixed $\omega = 0.04$ or 0.08 rad/s, the constitutive voltage-current relations are simulated and depicted in Fig. 2. As can be found, all the four DMs can display the initial-relied hysteresis loops pinched at the origin and their hysteresis loop lobe areas are closely related to the memristor initials. Consequently, the numerical results manifest that the presented four DMs can retain the properties of the continuous-time memristors [1]. In addition, the discrete memristance $M(q_n)$ changes along with the iterative sequence of the charge variable $q$ and its initial value.

### B. Unified DM Mapping Model and Four 2D DM Maps

Due to the special nonlinearities, the presented DMs in (3) can be used to generate four types of discrete maps. Here, we present a simplest implementation approach and its schematic structure is plotted in Fig. 3. After scaling by a proportional controller $k$, the iteration sequence generated by a DM is an output of the unified DM mapping model, and it is also used as an input of the model for next iteration. Using such a schematic structure, 2D DM maps can be easily constructed.

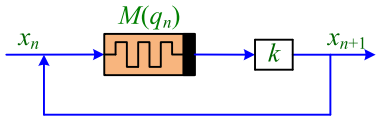


Fig. 3. The schematic structure of a unified DM mapping model.

TABLE I
EQUATIONS, NAMES, PARAMETERS AND INITIALS OF FOUR 2D DM MAPS

| DM equations | Map names | Parameters ($k$) | Initials ($x_0$, $q_0$) |
|---|---|---|---|
| $\begin{cases} x_{n+1} = k(q_n^2 - 1)x_n, \\ q_{n+1} = q_n + x_n. \end{cases}$ | Q-DM map | 1.78 | (−0.5, 0.5) |
| $\begin{cases} x_{n+1} = k(\lvert q_n \rvert - 1)x_n, \\ q_{n+1} = q_n + x_n. \end{cases}$ | A-DM map | 2.30 | (−0.8, 0.6) |
| $\begin{cases} x_{n+1} = k\sin(\pi q_n)x_n, \\ q_{n+1} = q_n + x_n. \end{cases}$ | S-DM map | 1.84 | (0.5, −0.6) |
| $\begin{cases} x_{n+1} = k(e^{-\cos \pi q_n} - 1)x_n, \\ q_{n+1} = q_n + x_n. \end{cases}$ | E-DM map | 2.66 | (−0.5, 0.4) |

With the schematic structure in Fig. 3, the mathematical equations of a unified DM mapping model can be described by

$$\begin{aligned} x_{n+1} &= kM(q_n)x_n, \\ q_{n+1} &= q_n + x_n, \end{aligned} \tag{4}$$

where $k$ is the only control parameter. The unified DM mapping model in (4) is a 2D discrete system and its nonlinearity relates only to the DM. Substituting the memristance nonlinearities of (3) into (4), four 2D DM maps are then yielded and summarized in Table I.

Note that the unified DM mapping model in (4) cannot be applied to all DMs due to its extremely simple schematic structure shown in Fig. 3. When an ideal DM is considered in (4), the bounded iteration of the unified DM mapping model depends entirely on the control parameter $k$, discrete memristance $M(q_n)$ and initial values ($x_0$, $q_0$). According to the experimental simulations, we finally choose the four ideal DMs described by (2) and (3) as examples for analysis.

### C. Infinite Fixed Points and Stability

The stability of a discrete map can be analyzed using its fixed points [34]. For the unified DM mapping model, its fixed points are the solutions of the equations $x_n = kM(q_n)x_n$ and $q_n = q_n + x_n$. Thus, the unified DM mapping model has infinite fixed points that is located on the $q$-axis [18] and these fixed points can be described by

$$E = (0, c), \tag{5}$$

TABLE II
NAMES, EIGENVALUES AND UNSTABLE REGIONS OF FOUR 2D DM MAPS

| Map names | Eigenvalues ($\lambda_2$) | Unstable regions |
|---|---|---|
| Q-DM map | $k(c^2-1)$ | $\lvert c\rvert<\sqrt{1-1/k},\ \lvert c\rvert>\sqrt{1+1/k}$ |
| A-DM map | $k(\lvert c\rvert-1)$ | $\lvert c\rvert<1-1/k,\ \lvert c\rvert>1+1/k$ |
| S-DM map | $k\sin(\pi c)$ | $(1/\pi)\arcsin(1/k)<\lvert c\rvert<1-(1/\pi)\arcsin(1/k)$ |
| E-DM map | $k(e^{-\cos\pi c}-1)$ | $(1/\pi)\arccos[-\ln(1-1/k)]<\lvert c\rvert<1$, $\lvert c\rvert<(1/\pi)\arccos[-\ln(1+1/k)]$ |

**For the S-DM and E-DM maps, only the unstable regions located in the primary interval $c \in [-1, 1]$ are given.*

where $c$ represents a real constant.

A discrete map's fixed point can show the stable or unstable state and its stability can be featured by the eigenvalues of the Jacobian matrix of the mapping model at that point. The Jacobian matrix can be written as

$$\boldsymbol{J}_E = \begin{bmatrix} kM(c) & 0 \\ 1 & 1 \end{bmatrix}. \tag{6}$$

Then the corresponding eigenvalues are easily gotten as

$$\lambda_1 = 1, \quad \lambda_2 = kM(c). \tag{7}$$

When the eigenvalues $\lambda_1$ and $\lambda_2$ of the fixed points are inside the unit circle, the mapping model is stable. When any one of the eigenvalues $\lambda_1$ and $\lambda_2$ are outside the unit circle, the mapping model is unstable. As can be obtained from (7), the eigenvalue $\lambda_1$ is always on the unit circle, whereas the eigenvalue $\lambda_2$ could be inside or outside the unit circle, totally depending on the $kM(c)$. For the four 2D DM maps, the corresponding unstable regions related to the eigenvalue $\lambda_2$ are obtained in Table II. The theoretical results demonstrate that all the four DM maps have the particularly striking property owning the infinite fixed points, and these fixed points are unstable or critically stable, depending on the control parameter $k$ and memristor initial $c$. Hence, the unified DM mapping model completely differs from the mapping models of most regular discrete maps [23], [24] and its initial-depended stability can lead to the emergence of multistability [19].

### *D. Memristor Initial-Boosting Mechanism*

Importantly, the S-DM and E-DM maps listed in Table I can exhibit the memristor initial-boosted behavior. Such behavior was found in a continuous system due to the utilization of memristors with cosine memductance [33]. Likewise, a DM with cosine memductance can also achieve the coexistence of bifurcations and attractors when the memristor initial state was cyclically switched with period $2\pi$ [19]. To investigate this dynamical mechanism, we rewrite the iteration equation forms of these two maps as

$$\text{S-DM map: } x_{n+1} = k\sin[\pi(q_0 + \sum_{l=1}^{n-1} x_l)]x_n, \tag{8a}$$

$$\text{E-DM map: } x_{n+1} = k\{e^{-\cos[\pi(q_0+\sum_{l=1}^{n-1} x_l)]} - 1\}x_n. \tag{8b}$$

For an integer $m$, define

$$q_0 = q_{00} + 2m, \tag{9}$$

where $q_{00}$ is a compensation value that satisfies the requirement

$$-1 < q_{00} + \sum_{l=1}^{n-1} x_l < 1. \tag{10}$$

There yields

$$\sin[\pi(q_0 + \sum_{l=1}^{n-1} x_l)] = \sin[\pi(q_{00} + \sum_{l=1}^{n-1} x_l)], \tag{11a}$$

$$\cos[\pi(q_0 + \sum_{l=1}^{n-1} x_l)] = \cos[\pi(q_{00} + \sum_{l=1}^{n-1} x_l)]. \tag{11b}$$

The theoretical results in (11) indicate the periodic property of the sinusoidal memristance in (3c) and exponential memristance in (3d).

The S-DM and E-DM maps given in (8) are periodic for the memristor initial $q_0$. This property can be demonstrated from the invariance of these two maps by the transformation in (9). In this way, the dynamics of the S-DM and E-DM maps are repeatedly boosted by the memristor initial $q_0$ with period 2. This dynamical behavior behaves like that appeared in the memristor-based continuous system [33]. Hence, the S-DM and E-DM maps are two boostable discrete maps caused by the memristor initials along the $q$-axis. The obvious benefit of this property is that the hyperchaotic attractors and their hyperchaotic sequences generated by the S-DM and E-DM maps can be boosted by switching their memristor initials.

## III. BIFURCATION PLOTS AND INITIAL-BOOSTED BEHAVIORS

This section studies the four 2D DM maps using multiple numerical measures, including the parameter-relied bifurcation behaviors, initials-relied coexisting behaviors, and memristor initial-boosted behaviors.

### *A. Parameter-Relied Bifurcation Behaviors*

To study the bifurcation behaviors of these four 2D DM maps, we set the parameter $k$ as a changeable parameter. Some typical initial values of each 2D DM map are selected and they are listed in Table I. As $k$ varies in the parameter intervals, the numerical plots of bifurcation diagrams (bottom) and Lyapunov exponents (LEs) (top) are depicted, as shown in Fig. 4. The typical initial values ($x_0$, $q_0$) and adjustable ranges of the parameter $k$ are tagged in details. All the LE values are calculated using the Wolf's Jacobian algorithm.

Observed from Fig. 4, all the four 2D DM maps can show hyperchaos. The A-DM map has the narrowest hyperchaos parameter interval, while the other three maps have relatively wide hyperchaos parameter intervals. As the increasement of the parameter $k$, all the four 2D DM maps undergo the period-doubling bifurcation route to chaos and present the dynamical behaviors of period, chaos, hyperchaos, and periodic windows. Note that each of the Q-DM, S-DM and E-DM maps has the widest periodic window with complex bifurcation behaviors,

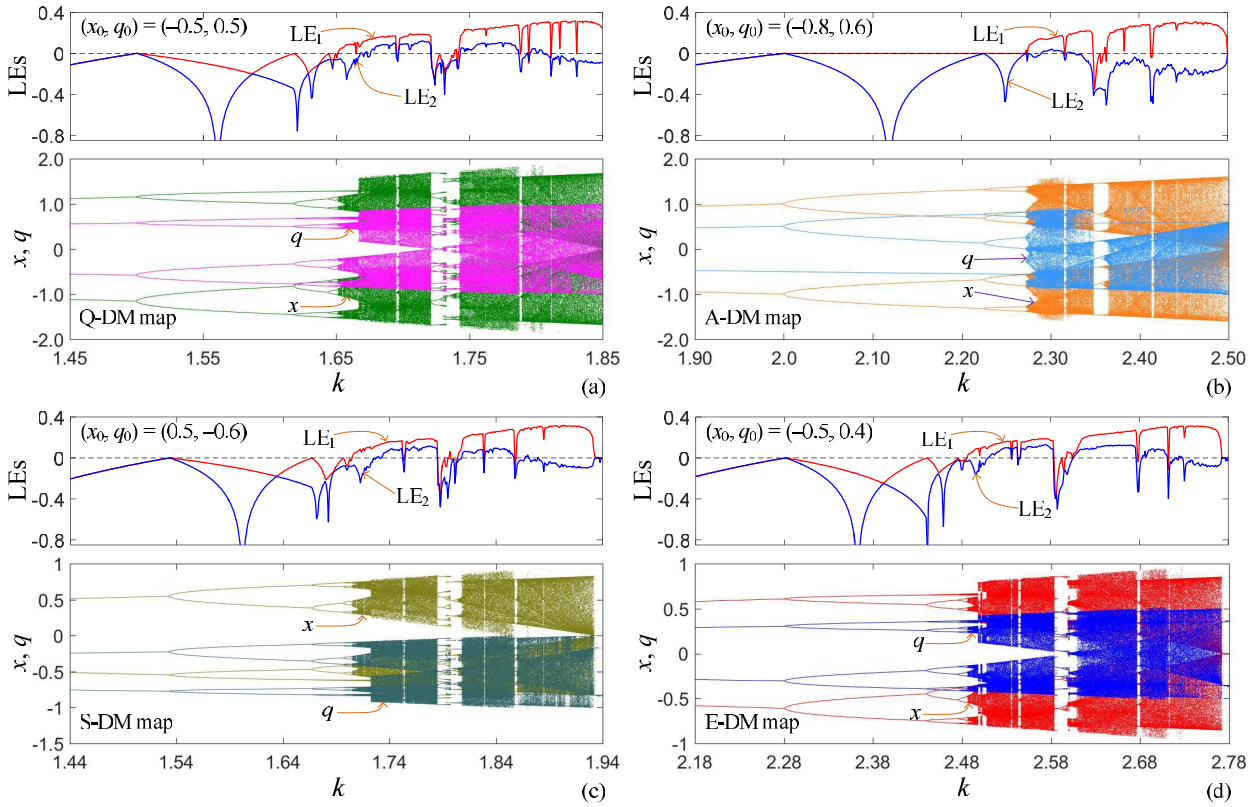


Fig. 4. For the four 2D DM maps, the parameter-relied bifurcation diagrams (bottom) and LEs (top). (a) For $(x_0, q_0) = (-0.5, 0.5)$, numerical plots of the Q-DM map with $k \in [1.45, 1.85]$. (b) For $(x_0, q_0) = (-0.8, 0.6)$, numerical plots of the A-DM map with $k \in [1.9, 2.5]$. (c) For $(x_0, q_0) = (0.5, -0.6)$, numerical plots of the S-DM map with $k \in [1.44, 1.94]$. (d) For $(x_0, q_0) = (-0.5, 0.4)$, numerical plots of the E-DM map with $k \in [2.18, 2.78]$.

including bifurcation break, state mutation and local self-similarity.

### *B. Initials-Relied Coexisting Behaviors*

The initials-relied multistability with the coexistence of multiple isolated attractors is a nature of most continuous and discrete dynamical systems [35], [36]. For a nonlinear system with multistability, its long-term dynamical behaviors are essentially different and depend on which basin of attraction the initial value belongs [35]. Such phenomenon of multistability can be easily emerged in a memristor-based dynamical system due to the introduction of the continuous or discrete memristor [17]–[19]. As can be seen from Table II, the infinite fixed points of the four 2D DM maps with the given parameters can be unstable or critically stable at different memristor initials. This situation can lead to the appearance of the stable point attractors in some initial regions of these 2D DM maps, which means that these maps can show bi-stability of coexisting attractors and have two kinds of basins of attraction.

To detect the bi-stable behaviors of coexisting attractors, the basins of attraction are used to divide the initial regions according to different long-term behaviors of the 2D DM maps.

For the Q-DM and A-DM maps, their basins of attraction are colored by measuring every initial value in the $x_0-q_0$ plane and the results are shown in Figs. 5(a1) and 5(b1). The black region stands for the hyperchaotic attractor (HCA) and the

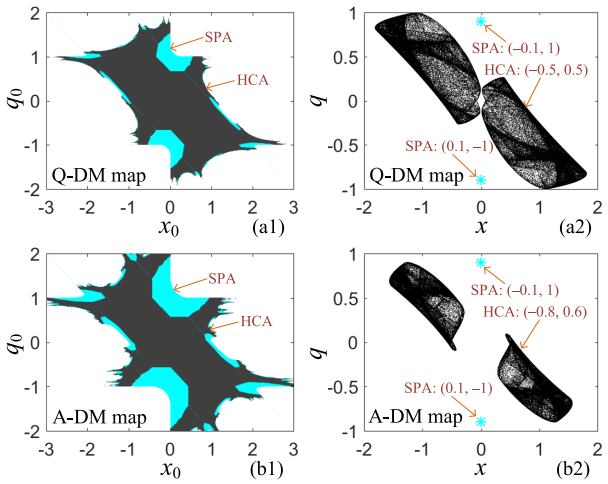


Fig. 5. Initials-relied coexisting behaviors in the Q-DM and A-DM maps with the typical parameters. (a) For the Q-DM map with $k = 1.78$, the basins of attraction (a1) and coexisting attractors (a2). (b) For the A-DM map with $k = 2.3$, the basins of attraction (b1) and coexisting attractors (b2).

cyan region indicates the stable point attractor (SPA). Note that the white region represents the unbounded divergent behavior. Thus, the bi-stability phenomenon of coexisting hyperchaotic and stable point attractors are disclosed in the Q-DM and A-DM maps. Interestingly, the region distributions of the two basins of attraction in Figs. 5(a1) and 5(b1) are symmetric about the antidiagonal line.

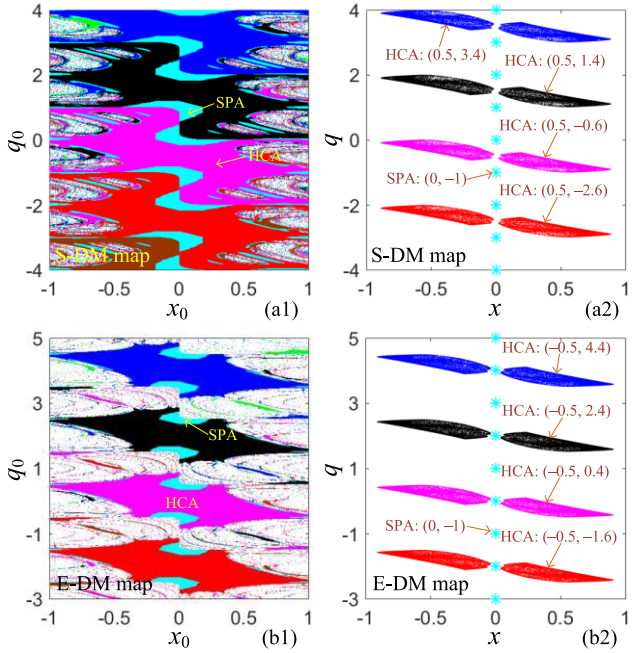


Fig. 6. Memristor initial-boosted behaviors in the S-DM and E-DM maps with the typical parameters. (a) For the S-DM map with $k = 1.84$, the basins of attraction (a1) and memristor initial-boosted attractors (a2). (b) For the E-DM map with $k = 2.66$, the basins of attraction (b1) and memristor initial-boosted attractors (b2).

Furthermore, Figs. 5(a2) and 5(b2) display the phase plane plots of coexisting attractors for the Q-DM and A-DM maps, respectively. The hyperchaotic attractors are triggered from the typical initials located in the black attraction regions of Figs. 5(a1) and 5(b1); whereas the two stable point attractors with different positions are initiated from $(-0.1, 1)$ and $(0.1, -1)$ respectively, all located in the cyan attraction regions of Figs. 5(a1) and 5(b1). The results confirm the emergences of bi-stability in these Q-DM and A-DM maps.

### C. Memristor Initial-Boosted Behaviors

According to the theoretical analysis in Section II-D, the S-DM and E-DM maps are two boostable maps and their dynamical behaviors are repeatedly boosted by memristor initials of $q_0$ with period 2. To exhibit such behaviors, the basins of attraction and phase plane plots are employed.

The parameters in the S-DM and E-DM maps are set as the typical values listed in Table I. To measure the dynamical effects of each initial value, we plot the basins of attraction of the S-DM and E-DM maps in the $x_0 - q_0$ plane and show the results in Figs. 6(a1) and 6(b1), respectively. In the basins of attraction, the blue, black, magenta, and red regions represent the HCAs with different offsets along the $q$-axis, the cyan regions represent the SPAs with different positions along the $q$-axis, and the white region represents the unbounded divergent behavior. As can be observed, the basins of attraction have complicated manifold structures and basin boundaries between the hyperchaos and stable point regions, and the main color blocks denote the four attraction regions of hyperchaotic attractors that have an offset with width 2 apart from each other. Such basins of attraction can embody the emergences of the bi-stability and memristor initial-boosted behaviors.

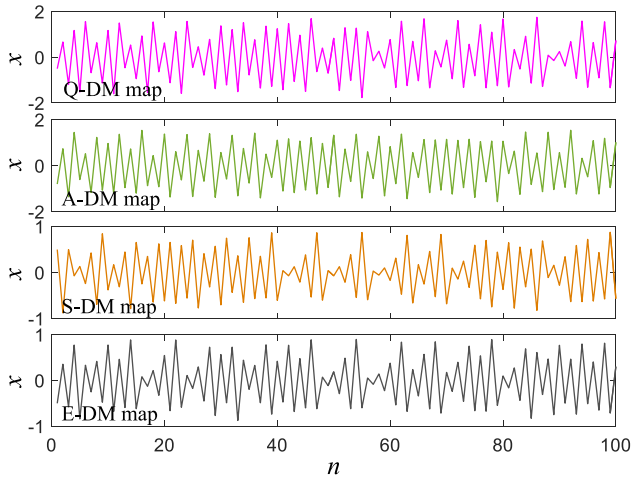


Fig. 7. Hyperchaotic sequences generated by the four DM maps under the typical parameters and initials listed in Table I.

Correspondingly, Figs. 6(a2) and 6(b2) depict the phase plane plots of the memristor initial-boosted coexisting attractors in the S-DM and E-DM maps, respectively. The hyperchaotic attractors marked by different colors are triggered from different initial values, which are located in the corresponding attraction regions marked by the same colors. The initials of the stable point attractors are located in the cyan attraction regions. The results in Fig. 6 manifest that the S-DM and E-DM maps can exhibit the boostable dynamical behaviors caused by the memristor initials. This boostable property makes the S-DM and E-DM maps more suitable for many chaos-based industrial applications [19].

## IV. Performance Analyses and Hardware Device

This section evaluates the performance indicators of hyperchaotic sequences generated by the four 2D DM maps and develops a hardware device to implement these hyperchaotic sequences.

### A. Hyperchaotic Sequences and Performance Analysis

The numerical simulations in the above section show that all the four 2D DM maps can generate hyperchaotic sequences. To quantitatively estimate their performance, we calculate their performance indicators including the LEs ($LE_1$, $LE_2$), spectral entropy (SE), permutation entropy (PE), correlation dimension (CorDim), and Kaplan-Yorke dimension ($D_{KY}$) [20]. The length of all these hyperchaotic sequences is set as 50000 for simplicity.

The parameters and initials are set as typical values listed in Table I and the generated hyperchaotic sequences of the four 2D DM maps are plotted in Fig. 7. As can be seen, they are all aperiodic and disordered. Correspondingly, the performance indicators of these hyperchaotic sequences are listed in Table III, which demonstrate that these hyperchaotic sequences all have excellent performance indicators. Note that the A-DM map has the slightly lower performance indicators than the other three maps.

It has been reported in many literatures that the chaotification or modulation mapping model can enhance the chaos

TABLE III
PERFORMANCE FOR HYPERCHAOTIC SEQUENCES OF FOUR DM MAPS

| DM maps | $LE_1$, $LE_2$ | SE | PE | CorDim | $D_{KY}$ |
|---|---|---|---|---|---|
| Q-DM map | 0.2692, 0.0925 | 0.9178 | 3.4519 | 1.5349 | 2.0000 |
| A-DM map | 0.1457, 0.0367 | 0.8355 | 3.3658 | 1.6685 | 2.0000 |
| S-DM map | 0.2554, 0.0972 | 0.9161 | 3.5426 | 1.5764 | 2.0000 |
| E-DM map | 0.2492, 0.1262 | 0.9104 | 3.5600 | 1.6057 | 2.0000 |

TABLE IV
PERFORMANCE COMPARISONS FOR CHAOTIC SEQUENCES OF SOME 2D MAPS

| Chaotic maps | Parameters | Initials | $LE_1$, $LE_2$ | SE | $D_{KY}$ |
|---|---|---|---|---|---|
| Q-DM map | 1.78 | (−0.5, 0.5) | 0.2692, 0.0925 | 0.9178 | 2.0000 |
| Hénon map | (1.4, 0.3) | (0, 0) | 0.4208, −1.6248 | 0.9276 | 1.2590 |
| Lozi map | (1.7, 0.5) | (0, 0) | 0.4701, −1.1632 | 0.9056 | 1.4041 |
| $CF_a$ map | (1.2, 2) | (0.27, 0.28) | 0.1344, −0.1383 | 0.8328 | 1.9718 |
| $NFI_a$ map | – | (0.93, −0.44) | 0.0599, −0.3223 | 0.2447 | 1.1860 |
| $NEM_1$ map | 2 | (1.7, −0.39) | 0.1167, −0.2679 | 0.8113 | 1.4358 |
| Sine map | (1.5, 3.8) | (−2, 1) | 0.5316, −0.7267 | 0.9347 | 1.7336 |

complexity of the existing discrete maps [15], [22]. To provide a fair performance comparison, we exclude all the chaotification or modulation maps. Taking the presented Q-DM map as an example, we compare its dynamical performance with that of six existing 2D chaotic maps under their typical parameter and initial settings and the results are listed in Table IV. These existing chaotic maps are the Hénon map [23], Lozi map [24], $CF_a$ map with curve fixed points [25], hidden $NFI_a$ map [26], $NEM_1$ quadratic map [27], and Sine boostable map [20].

One can see that only the presented Q-DM map owns two positive LEs and thus shows hyperchaos with $D_{KY} = 2$. As a contrast, all the existing 2D chaotic maps listed in Table IV have only one positive LE and display chaos with $D_{KY} < 2$. Meanwhile, the Q-DM map can achieve the relatively larger SE than most existing 2D chaotic maps. This demonsrtates that the Q-DM map has excellent chaos complexity. These comparative results declare that the hyperchaotic sequences generated by the four 2D DM maps have higher randomness and better unpredictability.

### *B. Initial-Controlled Hyperchaotic Sequences*

Observed from the memristor initial-boosted behaviors shown in Fig. 6, the memristor initial-controlled hyperchaotic sequences can be generated from the S-DM and E-DM maps with the typical parameters. The initial values for the S-DM map are set as $x_0 = 0.5$ and $q_0 = -0.6+2m(m = -1, 0, 1, 2)$, and those for the E-DM map are set as $x_0 = -0.5$ and $q_0 = 0.4 + 2m(m = -1, 0, 1, 2)$. Thus, two sets of four-way hyperchaotic sequences can be generated by the S-DM and E-DM maps and they are shown in Fig. 8. Notably, the hyperchaotic sequences generated by these two maps are boosted by the memristor initials with offset 2 along the $q$-axis. This indicates that the oscillation amplitudes of the hyperchaotic sequences can be non-destructively controlled by switching their memristor initials.

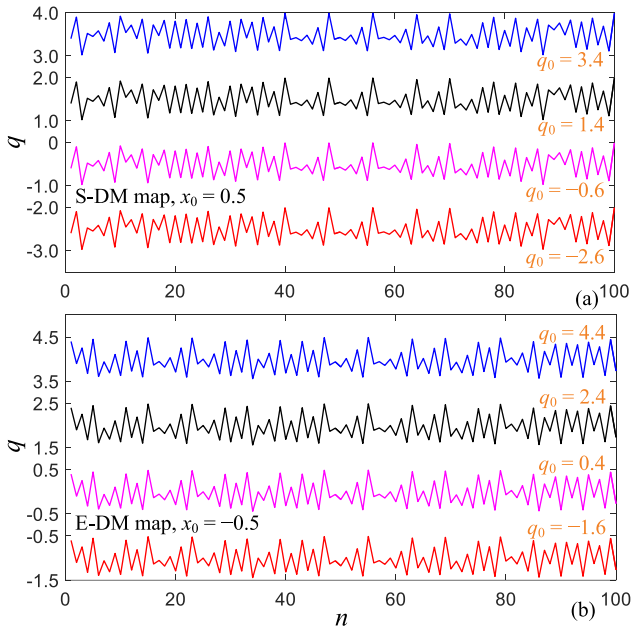


Fig. 8. Memristor initial-controlled hyperchaotic sequences of the S-DM and E-DM maps, reflecting the robust hyperchaos controlled by switching the memristor initials.

TABLE V
PERFORMANCE FOR HYPERCHAOTIC SEQUENCES OF S-DM AND E-DM MAPS

| DM maps | Initial Values | $LE_1$, $LE_2$ | SE | PE | CorDim |
|---|---|---|---|---|---|
| S-DM map | (0.5, 3.4) | 0.2568, 0.0922 | 0.9159 | 3.5362 | 1.4646 |
| | (0.5, 1.4) | 0.2583, 0.0955 | 0.9151 | 3.5370 | 1.5254 |
| | (0.5, −0.6) | 0.2554, 0.0972 | 0.9161 | 3.5426 | 1.5764 |
| | (0.5, −2.6) | 0.2543, 0.0925 | 0.9157 | 3.5356 | 1.4691 |
| E-DM map | (−0.5, 4.4) | 0.2503, 0.1280 | 0.9122 | 3.5762 | 1.6109 |
| | (−0.5, 2.4) | 0.2510, 0.1228 | 0.9104 | 3.5651 | 1.6157 |
| | (−0.5, 0.4) | 0.2492, 0.1262 | 0.9104 | 3.5600 | 1.6057 |
| | (−0.5, −1.6) | 0.2490, 0.1221 | 0.9117 | 3.5683 | 1.6103 |

The dynamical performance of the memristor initial- controlled hyperchaotic sequences generated by the S-DM and E-DM maps can be evaluated by employing the same performance indicators aforementioned and the evaluation results are shown in Table V. Note that since all the $D_{KY}$ values here are 2, they are not listed in the table. As can be seen from the table, these memristor initial-controlled hyperchaotic sequences have almost the same values for different performance indicators. Therefore, the hyperchaotic sequences of the S-DM and E-DM maps have high controllability by the memristor initials and the memristor initial-controlled hyperchaotic sequences are robust. Generally, the hyperchaotic/chaotic sequences of high-dimensional discrete maps have more excellent dynamical performance [37]. But these hyperchaotic/chaotic maps don't own this non-destructive control property.

### *C. Hardware Experiment Verification*

Here, we develop a hardware device to implement the four 2D DM maps using a microcontroller. The

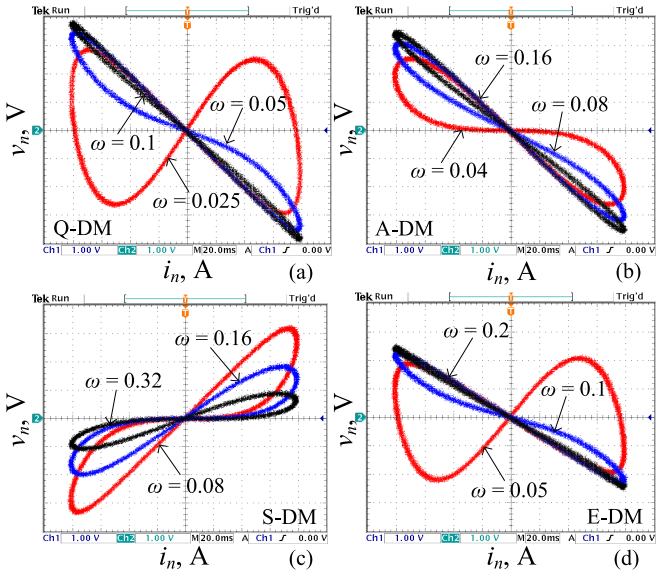


Fig. 9. The experimentally captured frequency-relied pinched hysteresis loops of four DMs when applying a discrete current source $i_n = 0.02\sin(\omega n)$ A, where the memristor initial is fixed as $q_0 = 0$ C and different radian frequencies of $\omega$ (rad/s) are given in the diagram. (a) Q-DM. (b) A-DM. (c) S-DM. (d) E-DM.

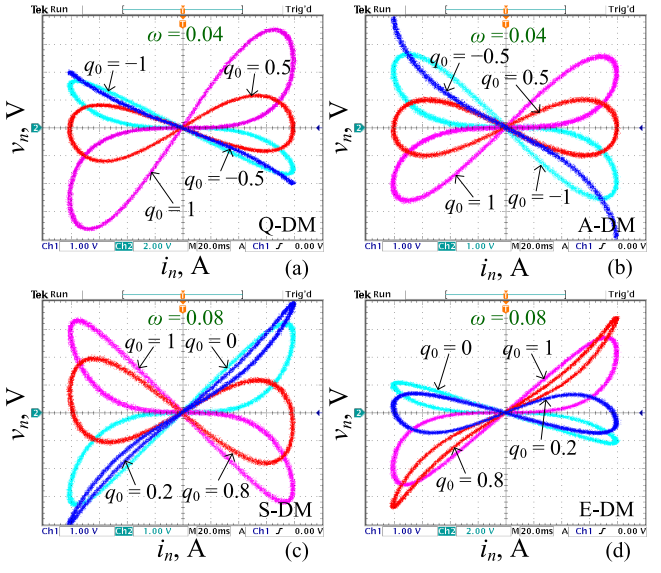


Fig. 10. The experimentally captured initial-relied pinched hysteresis loops of four DMs when applying a discrete current source $i_n = 0.02\sin(\omega n)$ A, where the memristor initial $q_0$ (C) and radian frequency $\omega$ (rad/s) are given in the diagram. (a) Q-DM. (b) A-DM. (c) S-DM. (d) E-DM.

experiment device consists of one high-performance 32-bit STM32F407VET6 microcontroller, two low-power 12-bit TLV5618 D/A converters, and other peripheral circuits. The microcontroller is used for implementing the four 2D DM maps, the D/A converters provide the analog voltage signals, and the peripheral circuits realize the voltage level conversion and output the results to the connected oscilloscope.

Based on the general model of ideal DM in (2) and the four representations of DMs in (3), four software DM cores are first programmed in C language, and then downloaded to the microcontroller. The parameters and initials for these DM cores are set based on the numerical results in Figs. 1 and 2 and the discrete current $i_n = 0.02\sin(\omega n)$ A is generated in C language. When fixing the memristor initial as $q_0 = 0$ C, Fig. 9 display the experimentally captured voltage-current loci for different values of $\omega$. And when fixing $\omega = 0.04$ or 0.08 rad/s, Fig. 10 shows the experimentally captured voltage-current loci for different values of memristor initial $q_0$. One can see that the four DM cores display the pinched hysteresis loops in the hardware device and the experimental results well confirm the numerical simulations.

Similarly, according to the mathematical representations of the four 2D DM maps listed in Table I, the software codes are programmed using the aforementioned four software DM cores and downloaded to the microcontroller. The settings of the parameters and initials are preloaded to the hardware device. When the supply power is turned on, the four-channel analog voltage signals can be synchronously captured by the oscilloscope. Fig. 11(a) shows the snapshot of the hardware device, and Fig. 11(b) demonstrates a set of four-channel analog voltage signals generated by the four 2D DM maps, where the settings of the parameters and initials are listed in Table I. Afterwards, Figs. 11(c) and 11(d) display two sets of four-channel analog voltage signals generated by the S-DM

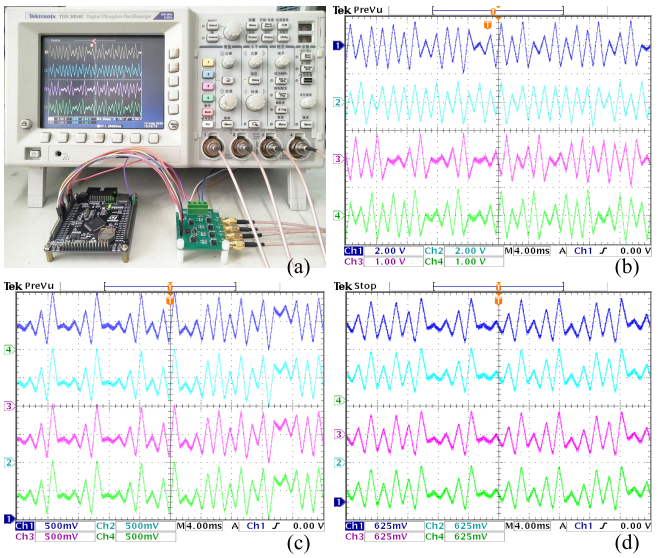


Fig. 11. Hardware device and hyperchaotic sequences. (a) Experimental prototype with the measured hyperchaotic sequences. (b) Hyperchaotic sequences generated by the four DM maps, the vertical is 2/2/1/1 V/div for $x$ and the horizontal is 4 ms/div for time. (c) Memristor initial-boosted hyperchaotic sequences of the S-DM map, the vertical is 500 mV/div for $q$ and the horizontal is 4 ms/div for time. (d) Memristor initial-boosted hyperchaotic sequences of the E-DM map, the vertical is 625 mV/div for $q$ and the horizontal is 4 ms/div for time.

and E-DM maps under four different memristor initials, where the parameter settings are listed in Table I and the initial values are listed in Table V. The experimental results show the feasibility and simplicity of the digitally microcontroller-based hardware implementation, and also manifest the generations of memristor initial-controlled robust hyperchaos in the hardware implementation.

The hardware device in this experiment is a digital circuit rather than an analog circuit. Certainly, the 2D DM maps can be implemented by some realistic devices in analog. For this

purpose, we need to construct some sampling switch-based memristor circuits with different memductance nonlinearities by referring to [18]. However, when implemented in some realistic devices, the memristor inner initial values cannot be set in advance so that the experimental measurements cannot be carried out effectively.

## V. Application in Pseudo-Random Number Generator

Thinks to many significant properties including the initial sensitivity and unpredictability, the chaotic systems have wide applications in many academic and industrial fields such as the pseudo-random number generator (PRNG) [38], [39]. In this section, to show the high performance of the four 2D DM maps in the PRNGs, we design four PRNGs using the four 2D DM maps and analyze the randomness of the generated pseudo-random numbers (PRNs).

### A. Design of PRNG

A simple PRNG is designed to show the application of these four 2D DM maps. Suppose a chaotic sequence $X = \{X(1), X(2), \ldots, X(n), \ldots\}$ is generated by one DM hyperchaotic map. First, convert each of the output $X(n)$ to be a 52-bit binary stream $X_B(n)$ using the IEEE 754 float standard, then the digital numbers from 35-th to 42-th in a binary stream are used as the PRNs, which can be presented as

$$P_i = X_B(n)_{35:42} \tag{12}$$

It is obvious that each output state of a chaotic map can generate 8 binary numbers. Here, we take the Q-DM and E-DM maps as two examples and the PRNGs using the Q-DM and E-DM maps are called QM-PRNG and EM-PRNG, respectively.

### B. NIST SP800-22 Test

A PRNG should generate PRNs with high randomness. To test the randomness of the proposed PRNGs, the National Institute of Standards and Technology (NIST) SP800-22 [40] is applied. It is a convinced and all-sided test standard that contains 15 sub-tests. Each sub-test is developed to find the non-randomness area of a set of binary sequences from various aspects. A significance level $\alpha$ in the NIST SP80-22 is used to measure the statistic errors and it is set as 0.01 in our experiments according to the recommendation in [40]. The length of each binary sequence should be larger than or at least equal to $10^6$ and the number of binary sequence should be larger than the inverse of the significance level, which is set as 120 in our experiment. Thus, our experiment generates a set of 120 binary sequences with $10^6$ length using each PRNG and tests the randomness of these binary sequences by the NIST SP00-22.

A test report is generated in the NIST SP800-22 test. Each sub-test can produce a P-value for each binary sequence. Then 120 P-values can be generated in each sub-test and the test result can be explained from two aspects: pass rate and P-value$_T$. The pass rate checks the proportion of the passed binary sequences. A binary sequence can pass a sub-test if its generated P-value is larger than or at least equals to the significance level. According to the discussion in [40], the minimum pass rate is 0.9628 when the significance level $\alpha = 0.01$ and the binary sequence number is 120. The P-value$_T$ calculates the distribution of the 120 P-values. First divide the interval [0, 1] into ten sub-intervals uniformly. Then count the number of the P-values within each sub-interval. Finally, a $\chi^2$ test is performed to the distribution of the P-values to obtain the P-value$_T$. The binary sequences are considered to pass the sub-test if the obtained P-value$_T$ is larger than 0.0001 [40]. Table VI lists the test results of the random numbers generated by different PRNGs in the NIST SP800-22 test. As can be seen, all the pass rates and P-value$_T$s generated by the QM-PRNG and EM-PRNG are all larger than 0.9628 and 0.0001, respectively. This indicates that the presented hyperchaotic maps can generate PRNs with high randomness. Note that to save space, we only list the test results of the PRNs generated by the Q-DM and E-DM maps. In fact, the PRNs generated by all the four DM maps can pass the test.

TABLE VI
NIST SP800-22 Test Results of the Random Numbers by Two PRNGs

| No. | Sub-tests | QM-PRNG | | EM-PRNG | |
|---|---|---|---|---|---|
| | | Pass rate | P-value$_T$ | Pass rate | P-value$_T$ |
| | | $\geq 0.9628$ | $\geq 0.0001$ | $\geq 0.9628$ | $\geq 0.0001$ |
| 01 | Frequency | 1.0000 | 0.0252 | 0.9917 | 0.6198 |
| 02 | Block Frequency | 0.9833 | 0.1413 | 0.9917 | 0.7887 |
| 03 | Cum. Sums* (F) | 0.9833 | 0.9705 | 0.9917 | 0.5510 |
| | Cum. Sums* (R) | 1.0000 | 0.2536 | 0.9917 | 0.9001 |
| 04 | Runs | 0.9833 | 0.9001 | 0.9917 | 0.7231 |
| 05 | Longest Runs | 0.9917 | 0.2993 | 0.9833 | 0.1952 |
| 06 | Rank | 0.9500 | 0.5009 | 0.9917 | 0.7887 |
| 07 | FFT | 0.9833 | 0.8623 | 1.0000 | 0.1952 |
| 08 | Non-Ovla. Temp.* | 0.9889 | 0.4968 | 0.9894 | 0.5308 |
| 09 | Ovla. Temp. | 0.9917 | 0.4686 | 0.9917 | 0.8881 |
| 10 | Universal | 0.9750 | 0.0119 | 0.9917 | 0.9001 |
| 11 | Appr. Entropy | 0.9917 | 0.6545 | 0.9833 | 0.9761 |
| 12 | Ran. Exc.* | 0.9833 | 0.4861 | 0.9819 | 0.3124 |
| 13 | Ran. Exc. Var.* | 0.9911 | 0.3825 | 0.9832 | 0.2596 |
| 14 | Serial (1st) | 0.9833 | 0.4373 | 0.9917 | 0.9885 |
| | Serial (2nd) | 0.9917 | 0.0704 | 1.0000 | 0.0571 |
| 15 | Linear complexity | 0.9833 | 0.0372 | 0.9917 | 0.4373 |
| | Success No. | 15/15 | 15/15 | 15/15 | 15/15 |

** Non-Ovla. Temp., Ran. Exc., and Ran. Exc. Var. tests are comprised of 148, 8, and 18 sub-tests, respectively. The average result of multiple sub-tests is reported.*

### C. Information Entropy Test

To compare the performance of the proposed DM maps with existing maps in generating PRNs, we separately use the four 2D DM maps in Table I and four existing 2D chaotic maps in Table IV as the source chaotic map in (12) to generate PRNs. To quantitatively evaluate the randomness of the generated PRNs, we measure the randomness using the information entropy.

TABLE VII
INFORMATION ENTROPY EVALUATIONS FOR THE PRNGS BY DIFFERENT MAPS

| 2D DM maps | Q-DM map | A-DM map | S-DM map | E-DM map |
|---|---|---|---|---|
| $H(P)$ | 7.8866 | 7.8835 | 7.8268 | 7.8587 |
| Existing 2D maps | Hénon map | $CF_a$ map | $NFI_a$ map | $NEM_1$ map |
| $H(P)$ | 7.8161 | 6.2698 | 6.5919 | 6.7802 |

The information entropy is a key performance indicator for measuring the distribution of a signal [41]. The information entropy of a signal $P$ can be described by

$$H(P) = -\sum_{i=1}^{2^n} p(P_i)\log_2 p(P_i), \tag{13}$$

where $P_i$ is the $i$-th possible value in $P$, $p(P_i)$ is the probability of $P_i$, and $n$ is the bit length in each value. In our experiment, each 8 bits of PRNs are set as a unit. Then the maximum value of information entropy is 8. A larger information entropy value implies the higher randomness of the PRNs generated by the chaotic map.

Table VII lists the information entropy values of different PRNs with 10,000-bit length generated by different PRNGs using different chaotic maps. The typical parameter and initial value settings of these chaotic maps are listed in Tables I and IV. As can be seen, the PRNs generated using the four 2D DM maps have higher information entropy values than that using the four existing 2D chaotic maps, which indicate that they have higher randomness. When PRNs are used in many applications, high randomness can achieve high performance. Thus, the PRNs generated using the four 2D DM maps can greatly promote the applications involving PRNs.

## VI. CONCLUSION

This paper reported four DMs and provided four 2D DM maps with different memductance nonlinearities. Due to the infinite fixed points, the four 2D DM maps can generate hyperchaos with coexisting bi-stable or memristor initial-boosted behavior. The hyperchaotic sequences generated by the S-DM and E-DM maps have the same performance indicators and their oscillating amplitudes can be non-destructively controlled by switching the memristor initials. This feature allows the S-DM and E-DM maps to suit many applications. Furthermore, a hardware device was developed to implement the four 2D DM maps using four software DM cores and the four-channel analog voltage signals were acquired. The hyperchaotic sequences generated by these 2D DM maps were used for designing PRNGs and the test experiments showed that these maps can generate PRNs with high randomness. Due to the excellent performance indictors, the generated hyperchaotic sequences can also be applied in many other applications such as the secure communication [42], image encryption [43], [44], and generative adversarial nets [45]. Meanwhile, the reported four DMs can also be applied to enhance the chaos complexity of existing discrete maps. These topics deserve further study.

## REFERENCES


[1] M. Chen, M. Sun, H. Bao, Y. Hu, and B. Bao, "Flux-charge analysis of two-memristor-based Chua's circuit: Dimensionality decreasing model for detecting extreme multistability," *IEEE Trans. Ind. Electron.*, vol. 67, no. 3, pp. 2197–2206, Mar. 2020.

[2] Z. Hua, B. Zhou, and Y. Zhou, "Sine chaotification model for enhancing chaos and its hardware implementation," *IEEE Trans. Ind. Electron.*, vol. 66, no. 2, pp. 1273–1284, Feb. 2019.

[3] X. Meng, P. Rozycki, J.-F. Qiao, and B. M. Wilamowski, "Nonlinear system modeling using RBF networks for industrial application," *IEEE Trans. Ind. Informat.*, vol. 14, no. 3, pp. 931–940, Mar. 2018.

[4] D. Abbasinezhad-Mood and M. Nikooghadam, "Efficient anonymous password-authenticated key exchange protocol to read isolated smart meters by utilization of extended Chebyshev chaotic maps," *IEEE Trans. Ind. Informat.*, vol. 14, no. 11, pp. 4815–4828, Nov. 2018.

[5] H.-T. Yau, S.-Y. Wu, C.-L. Chen, and Y.-C. Li, "Fractional-order chaotic self-synchronization-based tracking faults diagnosis of ball bearing systems," *IEEE Trans. Ind. Electron.*, vol. 63, no. 6, pp. 3824–3833, Jun. 2016.

[6] F. Corinto and M. Forti, "Memristor circuits: Bifurcations without parameters," *IEEE Trans. Circuits Syst. I, Reg. Papers*, vol. 64, no. 6, pp. 1540–1551, Jun. 2017.

[7] Z. Zeng, J. Wang, and X. Liao, "Global exponential stability of a general class of recurrent neural networks with time-varying delays," *IEEE Trans. Circuits Syst. I, Fundam. Theory Appl.*, vol. 50, no. 10, pp. 1353–1358, Oct. 2003.

[8] Z. Zeng and J. Wang, "Design and analysis of high-capacity associative memories based on a class of discrete-time recurrent neural networks," *IEEE Trans. Syst. Man, Cybern. B, Cybern.*, vol. 38, no. 6, pp. 1525–1536, Dec. 2008.

[9] L. O. Chua, "If it's pinched it's a memristor," *Semicond. Sci. Technol.*, vol. 29, no. 10, Sep. 2014, Art. no. 104001.

[10] M. Prezioso, F. Merrikh-Bayat, B. D. Hoskins, G. C. Adam, K. K. Likharev, and D. B. Strukov, "Training and operation of an integrated neuromorphic network based on metal-oxide memristor," *Nature*, vol. 521, no. 7550, pp. 61–64, 2015.

[11] P. Yao *et al.*, "Fully hardware-implemented memristor convolutional neural network," *Nature*, vol. 577, no. 7792, pp. 641–646, Jan. 2020.

[12] S. Chen, S. Yu, J. Lu, G. Chen, and J. He, "Design and FPGA-based realization of a chaotic secure video communication system," *IEEE Trans. Circuits Syst. Video Technol.*, vol. 28, no. 9, pp. 2359–2371, Sep. 2018.

[13] S. Vaidyanathan, V. T. Pham, and C. Volos, "Adaptive control, synchronization and circuit simulation of a memristor-based hyperchaotic system with hidden attractors," in *Advances in Memristors, Memristive Devices and Systems*. Cham, Switzerland: Springer, 2017, pp. 101–130.

[14] F. Yu *et al.*, "Chaos-based application of a novel multistable 5D memristive hyperchaotic system with coexisting multiple attractors," *Complexity*, vol. 2020, Mar. 2020, Art. no. 8034196.

[15] Z. Hua, Y. Zhou, and B. Bao, "Two-dimensional sine chaotification system with hardware implementation," *IEEE Trans. Ind. Informat.*, vol. 16, no. 2, pp. 887–897, Feb. 2020.

[16] B. C. Bao, H. Z. Li, L. Zhu, X. Zhang, and M. Chen, "Initial-switched boosting bifurcations in 2D hyperchaotic map," *Chaos, Interdiscipl. J. Nonlinear Sci.*, vol. 30, no. 3, Mar. 2020, Art. no. 033107.

[17] F. Corinto, M. Forti, and L. O. Chua, "Memristor circuits: Invariant manifolds, coexisting attractors, extreme multistability, and bifurcations without parameters," in *Nonlinear Circuits and Systems With Memristors*. Cham, Switzerland: Springer, 2021, pp. 219–269.

[18] B. Bao, H. Li, H. Wu, X. Zhang, and M. Chen, "Hyperchaos in a second-order discrete memristor-based map model," *Electron. Lett.*, vol. 56, no. 15, pp. 769–770, Jul. 2020.

[19] H. Li, Z. Hua, H. Bao, L. Zhu, M. Chen, and B. Bao, "Two-dimensional memristive hyperchaotic maps and application in secure communication," *IEEE Trans. Ind. Electron.*, early access, Sep. 15, 2021, doi: 10.1109/TIE.2020.3022539.

[20] H. Bao, Z. Hua, N. Wang, L. Zhu, M. Chen, and B. Bao, "Initials-boosted coexisting chaos in a 2-D sine map and its hardware implementation," *IEEE Trans. Ind. Informat.*, vol. 17, no. 2, pp. 1132–1140, Feb. 2021.

[21] C. Li, B. Feng, S. Li, J. Kurths, and G. Chen, "Dynamic analysis of digital chaotic maps via state-mapping networks," *IEEE Trans. Circuits Syst. I, Reg. Papers*, vol. 66, no. 6, pp. 2322–2335, Jun. 2019.

[22] Z. Hua, Y. Zhou, C.-M. Pun, and C. L. P. Chen, "2D sine logistic modulation map for image encryption," *Inf. Sci.*, vol. 297, pp. 80–94, Mar. 2015.

[23] M. Hénon, "A two-dimensional mapping with a strange attractor," *Commun. Math. Phys.*, vol. 50, no. 1, pp. 69–77, Feb. 1976.
[24] V. Botella-Soler, J. M. Castelo, J. A. Oteo, and J. Ros, "Bifurcations in the Lozi map," *J. Phys. A, Math. Theor.*, vol. 44, no. 30, Jun. 2011, Art. no. 305101.
[25] H. Jiang, Y. Liu, Z. Wei, and L. Zhang, "A new class of two-dimensional chaotic maps with closed curve fixed points," *Int. J. Bifurcation Chaos*, vol. 29, no. 7, Jun. 2019, Art. no. 1950094.
[26] H. Jiang, Y. Liu, Z. Wei, and L. Zhang, "Hidden chaotic attractors in a class of two-dimensional maps," *Nonlinear Dyn.*, vol. 85, no. 4, pp. 2719–2727, Sep. 2016.
[27] S. Panahi, J. C. Sprott, and S. Jafari, "Two simplest quadratic chaotic maps without equilibrium," *Int. J. Bifurcation Chaos*, vol. 28, no. 12, Nov. 2018, Art. no. 1850144.
[28] D. B. Strukov, G. S. Snider, D. R. Stewart, and R. S. Williams, "The missing memristor found," *Nature*, vol. 453, no. 7191, pp. 80–83, May 2008.
[29] D. Batas and H. Fiedler, "A memristor SPICE implementation and a new approach for magnetic flux-controlled memristor modeling," *IEEE Trans. Nanotechnol.*, vol. 10, no. 2, pp. 250–255, Mar. 2011.
[30] H. Kim, M. P. Sah, C. Yang, S. Cho, and L. O. Chua, "Memristor emulator for memristor circuit applications," *IEEE Trans. Circuits Syst. I, Reg. Papers*, vol. 59, no. 10, pp. 2422–2431, Oct. 2012.
[31] B. Bao, J. Yu, F. Hu, and Z. Liu, "Generalized memristor consisting of diode bridge with first order parallel RC filter," *Int. J. Bifurcation Chaos*, vol. 24, no. 11, Nov. 2014, Art. no. 1450143.
[32] H. Bao, N. Wang, B. Bao, M. Chen, P. Jin, and G. Wang, "Initial condition-dependent dynamics and transient period in memristor-based hypogenetic jerk system with four line equilibria," *Commun. Nonlinear Sci. Numer. Simul.*, vol. 57, pp. 264–275, Apr. 2018.
[33] H. Bao, M. Chen, H. Wu, and B. Bao, "Memristor initial-boosted coexisting plane bifurcations and its extreme multi-stability reconstitution in two-memristor-based dynamical system," *Sci. China Technol. Sci.*, vol. 63, no. 4, pp. 603–613, Apr. 2020.
[34] Z. Zeng, J. Wang, and X. Liao, "Stability analysis of delayed cellular neural networks described using cloning templates," *IEEE Trans. Circuits Syst. I, Reg. Papers*, vol. 51, no. 11, pp. 2313–2324, Nov. 2004.
[35] A. N. Pisarchik and U. Feudel, "Control of multistability," *Phys. Rep.*, vol. 540, no. 4, pp. 167–218, Jul. 2014.
[36] Z. Zeng and J. Wang, "Multiperiodicity of discrete-time delayed neural networks evoked by periodic external inputs," *IEEE Trans. Neural Netw.*, vol. 17, no. 5, pp. 1141–1151, Sep. 2006.
[37] Y. Wu, Z. Hua, and Y. Zhou, "N-dimensional discrete cat map generation using Laplace expansions," *IEEE Trans. Cybern.*, vol. 46, no. 11, pp. 2622–2633, Nov. 2018.
[38] C. Li, K. Tan, B. Feng, and J. Lü, "The graph structure of the generalized discrete Arnold's cat map," *IEEE Trans. Comput.*, early access, Jan. 13, 2021, doi: 10.1109/TC.2021.3051387.
[39] M. Bakiri, C. Guyeux, J.-F. Couchot, L. Marangio, and S. Galatolo, "A hardware and secure pseudorandom generator for constrained devices," *IEEE Trans. Ind. Informat.*, vol. 14, no. 8, pp. 3754–3765, Aug. 2018.
[40] A. L. Rukhin *et al.*, "A statistical test suite for random and pseudorandom number generators for cryptographic applications," Nat. Inst. Standards Technol., Gaithersburg, MD, USA, Special Publication 800-22 Revision 1a, Apr. 2010.
[41] N. Wang, C. Li, H. Bao, M. Chen, and B. Bao, "Generating multi-scroll Chua's attractors via simplified piecewise-linear Chua's diode," *IEEE Trans. Circuits Syst. I, Reg. Papers*, vol. 66, no. 12, pp. 4767–4779, Dec. 2019.
[42] L. Zhang, Z. Chen, W. Rao, and Z. Wu, "Efficient and secure noncoherent OFDM-based overlapped chaotic chip position shift keying system: Design and performance analysis," *IEEE Trans. Circuits Syst. I, Reg. Papers*, vol. 67, no. 1, pp. 309–321, Jan. 2020.
[43] Y. Ma, C. Li, and B. Ou, "Cryptanalysis of an image block encryption algorithm based on chaotic maps," *J. Inf. Secur. Appl.*, vol. 54, Oct. 2020, Art. no. 102566.
[44] A. Mansouri and X. Wang, "A novel one-dimensional sine powered chaotic map and its application in a new image encryption scheme," *Inf. Sci.*, vol. 520, pp. 46–62, May 2020.
[45] M. Naruse, T. Matsubara, N. Chauvet, K. Kanno, T. Yang, and A. Uchida, "Generative adversarial network based on chaotic time series," *Sci. Rep.*, vol. 9, no. 1, Sep. 2019, Art. no. 12963.

**Han Bao** received the B.S. degree in landscape design from the Jiangxi University of Finance and Economics, Nanchang, China, in 2015, and the M.S. degree in art and design from Changzhou University, Changzhou, China, in 2018. He is currently pursuing the Ph.D. degree in nonlinear system analysis and measurement technology with the Nanjing University of Aeronautics and Astronautics, Nanjing, China.

In 2019, he visited the Computer Science Department, The University of Auckland, New Zealand. His research interests include memristive neuromorphic circuit, nonlinear circuits and systems, and artificial intelligence.

**Zhongyun Hua** (Member, IEEE) received the B.S. degree from Chongqing University, Chongqing, China, in 2011, and the M.S. and Ph.D. degrees from the University of Macau, Macau, China, in 2013 and 2016, respectively, all in software engineering.

He is currently an Associate Professor with the School of Computer Science and Technology, Harbin Institute of Technology, Shenzhen, Shenzhen, China. His research interests include chaotic systems, chaos-based applications, multimedia security, and data hiding.

**Houzhen Li** (Graduate Student Member, IEEE) received the B.S. degree in optoelectronic information science and engineering from the Changshu Institute of Technology, Suzhou, China, in 2019. He is currently pursuing the M.S. degree in electronics science and technology with the School of Microelectronics and Control Engineering, Changzhou University, Changzhou, China. His research interests include memristive neuromorphic circuit and nonlinear circuits and systems.

**Mo Chen** (Member, IEEE) received the B.S. degree in information engineering, and the M.S. and Ph.D. degrees in electromagnetic field and microwave technology from Southeast University, Nanjing, China, in 2003, 2006, and 2009, respectively.

From 2009 to 2013, she was a Lecturer with Southeast University. She is currently an Associate Professor with the School of Microelectronics and Control Engineering, Changzhou University, Changzhou, China. Her research interests include memristor and its application circuits, and other nonlinear circuits and systems.

**Bocheng Bao** (Member, IEEE) received the B.S. and M.S. degrees in electronic engineering from the University of Electronic Science and Technology of China, Chengdu, China, in 1986 and 1989, respectively, and the Ph.D. degree in information and communication engineering, from the Nanjing University of Science and Technology, Nanjing, China, in 2010.

He has more than 20 year experience in the industry. He was with several enterprises as a senior engineer and the general manager. From 2008 to 2011, he was a Professor with the School of Electrical and Information Engineering, Jiangsu University of Technology, Changzhou, China. He was a Full Professor with the School of Microelectronics and Control Engineering, Changzhou University, Changzhou. In 2013, he visited the Department of Electrical and Computer Engineering, University of Calgary, Calgary, AB, Canada. His research interests include bifurcation and chaos, analysis and simulation in neuromorphic circuits, power electronic circuits, and nonlinear circuits and systems.

Dr. Bao was a recipient of the IET Premium Award in 2018 and selected as the Highly Cited Researcher 2020 in Cross-Field.